Identification of a core module for bone mineral density through the integration of a co-expression network and GWAS data

Olivia L Sabik [1,2], Gina M Calabrese[1], Eric Taleghani[1], Cheryl L Ackert-Bicknell[3], Charles R Farber*[1,4]

[1]Center for Public Health Genomics, School of Medicine, University of Virginia, Charlottesville, VA 22908
[2]Department of Biochemistry and Molecular Genetics, School of Medicine, University of Virginia, Charlottesville, VA 22908
[3]Center for Musculoskeletal Research, University of Rochester Medical Center, University of Rochester, Rochester, NY 14624
[4]Department of Public Health Sciences, University of Virginia, Charlottesville, VA 22908

Correspondence to: **Charles R. Farber**
E-mail: **crf2s@virginia.edu**
Center for Public Health Genomics
University of Virginia
P.O. Box 800717
Charlottesville, VA 22908, USA
Tel. 434-243-8584

Present Address for Dr. Cheryl Ackert-Bicknell:
Department of Orthopedics
University of Colorado Hospital
Aurora, CO, USA

Abstract

Recently, the “omnigenic” model of the genetic architecture of complex traits proposed two general categories of causal genes, core and peripheral. Core genes are hypothesized to play a direct role in regulating disease; thus, their identification has the potential to reveal critical regulators and novel therapeutic targets. Here, we sought to identify genes with “core-like” characteristics for bone mineral density (BMD), one of the most significant predictors of osteoporotic fracture. This was accomplished by analyzing genome-wide association study (GWAS) data through the lens of a cell-type and timepoint-specific gene co-expression network for mineralizing osteoblasts. We identified a single co-expression network module that was enriched for genes implicated by GWAS and partitioned BMD heritability, correlated with *in vitro* osteoblast mineralization, and enriched for genes, which when mutated in humans or mice, led to a skeletal phenotype. Further characterization of this module identified four novel genes (*B4GALNT3*, *CADM1*, *DOCK9*, and *GPR133*) located within BMD GWAS loci with colocalizing expression quantitative trait loci (eQTL) and altered BMD in mouse knockouts, suggesting they are causal genetic drivers of BMD in humans. Our network-based approach identified a “core” module for BMD and provides a resource for expanding our understanding of the genetics of bone mass.

Introduction:

Osteoporosis is a disease characterized by low bone mineral density (BMD) and an increased risk of fracture [1]. Worldwide, it is one of the most common diseases, affecting over 200 million individuals and causing 8.9 million fractures annually [2]. Although osteoporosis is a multifactorial disease influenced by both environmental and genetic variation, fracture-related traits, such as BMD, are influenced, in large part, by genetics (h^2>0.5) [3–5]. Over the last decade large-scale genome wide association studies (GWASs) have begun to dissect the genetics basis of bone traits with a primary focus on BMD [6,7] . These studies have been tremendously successful, identifying over 1100 independent BMD associations [8–10]. However, despite the wealth of genetic signals, the genes and mechanisms through which these associations impact bone remain largely unknown [6,7].

Recently, the “omnigenic model” was proposed as a framework for understanding the genetic architecture of complex traits, such as BMD [11,12]. The model posits that all genes expressed in disease-relevant cell-types have the potential to contribute to disease variation. One of the key concepts of the omnigenic model is the classification of causal genes as either “core” or “peripheral”. Core genes are predicted to directly modulate traits; whereas, peripheral genes are expected to impact traits via their effects on networks of core genes [12]. The distinction between core and peripheral genes is logical given the evidence demonstrating that the contributions of genes to a disease or phenotype are not equal. As an example, *RUNX2* is a transcription factor and master regulator of osteoblast activity and bone formation that initiates a transcriptional program absolutely required for the formation of a mineralized skeleton [13]. In contrast, hundreds of genes have been identified participating in myriad pathways whose absence has subtle, often context-dependent (such as age and sex), effects on bone [8,9,14]. Furthermore, we know the same distinction lies in biological processes, some of which play an intimate role in the regulation of a trait, while others play minor accessory roles. Thus, the identification of causal genes from GWAS data and the labeling of such genes as core or

peripheral has the potential to highlight previously undiscovered key regulatory genes for specific trait-related biological processes, which may be more ideal therapeutic targets.

There are two main challenges in the identification of core genes. The first is how to precisely define them [12,15–17]. In the omnigenic model, a gene is defined as a "core" gene "if and only if the gene product (protein, or RNA for a noncoding gene) has a direct effect—not mediated through regulation of another gene—on cellular and organismal processes leading to a change in the expected value of a particular phenotype" [11,12]. This statistical definition is convenient for explaining the omnigenic model, but is difficult to utilize for the identification of core genes in practice. It is also very strict; e.g. is *RUNX2,* as described above, a core gene for BMD? Instead we propose to use a set of biologically motivated criteria to distinguish genes with core-like properties from those that are likely peripheral by leveraging known pathways and processes that are essential to a disease-associated trait. For example, we would expect the expression of genes with core-like properties operating in pathways of critical importance in the regulation of BMD to be correlated with BMD and their severe perturbation to have a substantial impact on BMD (e.g., monogenic disease genes).

The second challenge is designing a strategy to identify genes with core-like properties, since GWAS alone is incapable of determining whether a locus is driven by a core or peripheral gene. One of the primary tenets of the omnigenic model is that peripheral genes account for a substantial component of the heritability of a trait because their effects are amplified by interactions with networks of co-expressed core genes [12]. If one expects core genes to be co-expressed then integrating the results of GWAS with co-expression networks, which reflect the transcriptional programs associated with the trait of interest, is a logical approach to identify modules of genes with core-like properties. A number of studies have already successfully used co-expression networks to inform GWAS, however this approach has not been used in the context of the omnigenic model [18–22].

Here, we combine weighted gene co-expression network analysis (WGCNA) and BMD

GWAS data to identify genes that are causal genetic drives of BMD with core-like properties. Our approach used a co-expression network for mature, mineralizing osteoblasts which we hypothesized would allow us to identify core genes specific for the process of mineralization. We first identified network modules enriched for genes implicated by GWAS and partitioned BMD heritability and then used the following biologically motivated filters to identify modules enriched for genes with core-like properties (i.e. “core” modules): (1) correlation with *in vitro* mineralization (a process of fundamental importance to BMD), (2) enrichment for genes that, when knocked-out in mice, alter BMD, and (3) enrichment for monogenic skeletal disease genes. Our analysis identified a single module (referred to as the “purple” module) fulfilling all the proposed criteria of a core module. As would be expected of a core module for mineralization, the purple module was enriched for genes with well-known roles in osteoblast activity and bone formation. Furthermore, we identified two submodules of genes within the purple module that followed distinct patterns of expression across osteoblast differentiation, the early and the late differentiation submodule (EDS and LDS). We found that the LDS, relative to the EDS, was more enriched for genes with core-like properties. Supporting the hypothesis that many LDS genes are causal genetic drivers, we observed that lead BMD SNPs located in GWAS loci harboring an LDS gene were more likely to overlap active regulatory elements in osteoblasts. Further characterization of the LDS identified four novel genes (*B4GALNT3*, *CADM1*, *DOCK9*, and *GPR133)* located within BMD GWAS loci that had colocalizing human eQTL and altered BMD in mouse knockout studies. We anticipate that this integrative approach will aid in the search for genes with core-like properties and pathways underlying BMD and risk of fracture.

Results

I. Construction of a co-expression network reflecting transcriptional programs in mineralizing osteoblasts

The goal of this work was to use a cell- and stage-specific co-expression network to identify genes with core-like properties that are causal for BMD GWAS associations. We chose to focus on generating a co-expression network using transcriptomic data from a single cell-type at a single-time point during differentiation: mature, mineralizing osteoblasts. We hypothesized this would allow us to focus on genes with core-like properties in the context of mineralization, a process critical in the regulation of BMD. We began by using WGCNA to construct a co-expression network using transcriptomic profiles generated from mineralizing primary calvarial osteoblasts from 42 strains of Collaborative Cross (CC) mice [23]. The CC is a panel of genetically diverse recombinant inbred strains. The resulting network consisted of 65 modules of genes, with an average of 292 genes per module (**Figure 1 and Supplemental File 1**). Each co-expression module was distinguished by its assigned color (e.g., the purple module).

To confirm that modules of genes produced by the co-expression analysis represented transcriptional programs reflecting specific biological processes, we assessed whether modules were enriched for genes associated with specific gene ontology (GO) terms [24]. Most network modules were enriched for general biological processes, such as the immune response (P_{adj} = 6.6×10^{-36}) in the blue module, mRNA metabolism ($P_{adj} = 7.8 \times 10^{-9}$) in the darkolivegreen module, and chromatin remodeling ($P_{adj} = 1.9 \times 10^{-4}$) in the grey60 module (**Figure 1 and Supplemental File 2**). However, as would be expected, there were a subset of modules enriched for genes involved in the activity of osteoblasts. For example, the cyan module was enriched for members of the Wnt signaling pathway (a key regulator of osteoblast activity) (P_{adj} = 2.3×10^{-4}), the turquoise module was enriched for genes encoding extracellular matrix proteins ($P_{adj} = 3.5 \times 10^{-25}$) (such as genes encoding for collagens ($P_{adj} = 0.4 \times 10^{-10}$)), and the purple module was enriched for genes involved in skeletal system development ($P_{adj} = 2.3 \times 10^{-10}$) and osteoblast differentiation ($P_{adj} = 2.0 \times 10^{-6}$) (**Figure 1 and Supplemental File 2**). Given that network modules represented distinct biological processes, including those involved in mineralization and osteoblast activity, we were confident it would provide a platform for

identifying core genes related to mineralization that potentially underlie BMD GWAS associations.

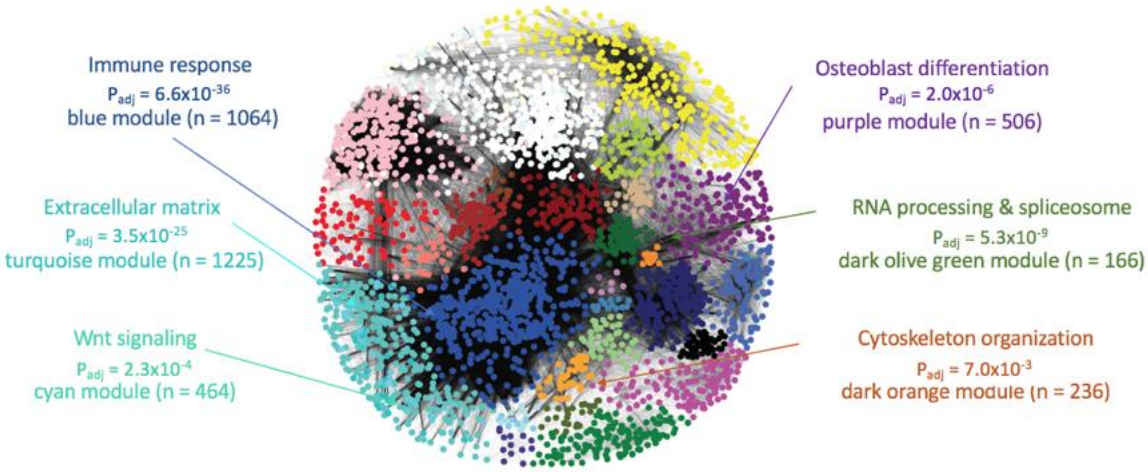

Figure 1. *Weighted gene co-expression network generated using transcriptomic profiles from mineralizing osteoblasts.* The network was composed of 65 modules of co-expressed genes, many of which were enriched for specific biological processes relevant to osteoblasts.

II. Identification of co-expression modules enriched for genes implicated by GWAS

To identify modules of co-expressed genes informative for GWAS, we first determined if any of the 65 modules were enriched for genes that overlapped GWAS associations. Using data from the two largest GWASs performed at the time, one study of Dual Energy X-Absorptiometry (DEXA) derived areal BMD measures at the lumbar spine and femoral neck [8] ("Estrada *et al.* GWAS"; N=32,961) and one study of ultrasound determined heel estimated BMD (eBMD) [9] ("Kemp *et al.* GWAS", N=142,487), we developed a list of 789 human genes ($N_{Estrada}$ = 179, N_{Kemp} = 701, (91 shared genes)) intersecting BMD GWAS loci. A total of 723 (92%) of these had mouse homologs in the network (**Supplemental File 3 and 4**). Of the 65 modules in the network, 13 were enriched for mouse homologs of human genes implicated by BMD GWAS (Fisher's exact test, $P_{adj} < 0.05$) (**Supplemental File 5 and Figure 2A**). Additionally, we

193 performed stratified LD score regression by calculating the BMD heritability partitioned by SNPs
194 surrounding genes in each module using the Kemp *et al.* GWAS [9,25]. We found 16 modules
195 enriched for partitioned BMD heritability, including nine of the 13 enriched for BMD GWAS
196 implicated genes (**Figure 2B and Supplemental File 6**).
197
198 **III. The purple module is enriched for genes with core-like properties**
199 Next, we focused on identifying which of the 13 modules identified above were enriched
200 for genes with core-like properties. To accomplish this, we selected modules using biologically
201 motivated criteria which likely reflected the properties of core genes. First, we compared the 13
202 module eigengenes with *in vitro* mineralization using osteogenic cultures from the same 42 CC
203 strains used in the construction of the co-expression network (**Supplemental Figure 1)**. Only
204 one, the purple module, had a pattern of expression that was significantly correlated with
205 mineralization (r = 0.49, P_{adj} = 0.012), suggesting the purple module was enriched for genes
206 with a direct role in mineralization (**Figure 2C and Supplemental Figure 2**).
207 Core genes have been broadly defined as those that directly influence a disease-
208 relevant biological processes [11,12]. Thus, severe perturbation of a core gene is more likely to
209 result in a significant impact on a phenotype, as in the case of a mouse knockout or human
210 monogenic disease. We identified all gene knockouts that produced a bone phenotype, defined
211 as either a change in BMD, bone mineral content (BMC), abnormal bone morphology, or
212 abnormal bone cell activity, by utilizing mouse knockout phenotype data from several databases
213 [26–29] (**Supplemental File 7**). Of the 13 modules enriched for BMD GWAS genes, two were
214 enriched for genes whose deficiency impacted bone in mice (**Figure 2D**). The purple module
215 was the most significantly enriched (OR=5.4, $P_{adj} = 1.6 \times 10^{-34}$). We also compiled a list of 35
216 known drivers of monogenic bone diseases associated with osteoblast dysfunction, including
217 osteogenesis imperfecta, hyperostosis, and osteosclerosis (**Supplemental File 8**) [30–34]. Again,
218 the purple module, containing 11 of 35 (31.4%) monogenic disease genes, was the most

219 significantly enriched (OR = 21.3, Padj = 6.9 x 10^{-9}) (**Figure 2E**). Together, these independent
220 lines of evidence suggested the purple module was enriched for genes with core-like properties.
221

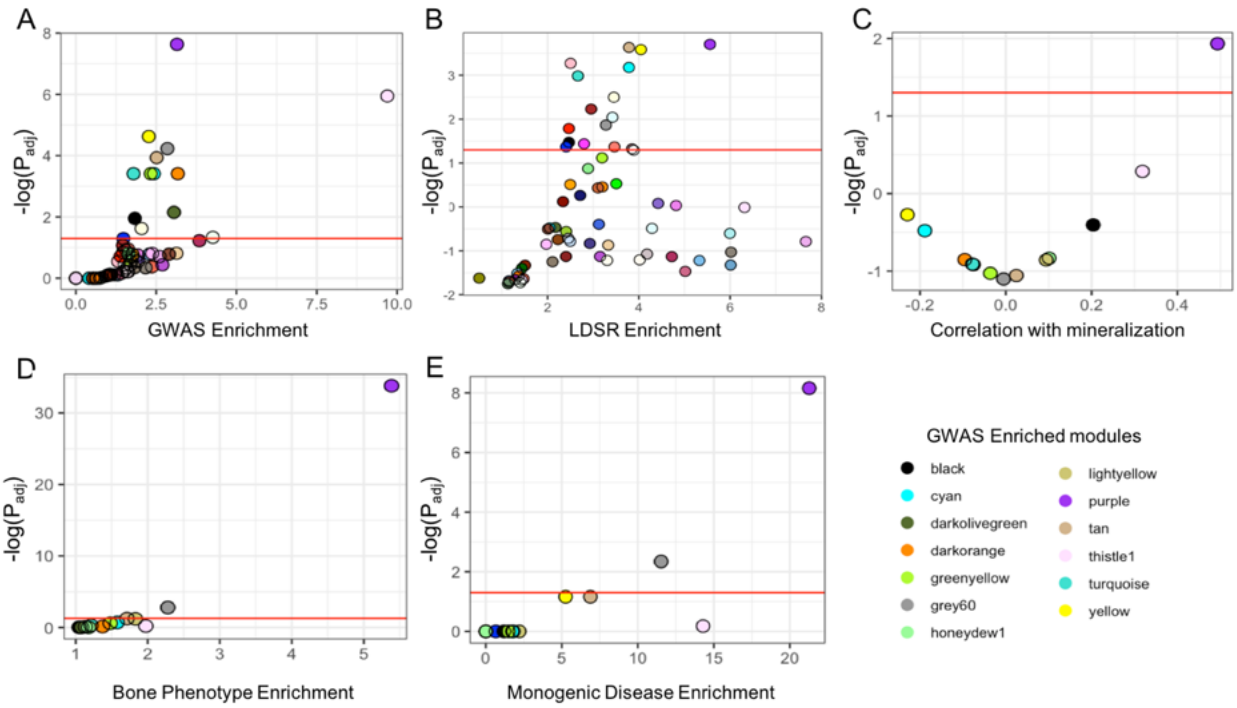

222

223 ***Figure 2.*** *The purple module is enriched for genes with core-like properties.* (A) Module
224 enrichments for genes overlapping a BMD GWAS association. (B) Enrichments for partitioned
225 BMD heritability for each module determined using stratified LD score regression. (C)
226 Correlation between each module eigengene and *in vitro* mineralization. (D) Module
227 enrichments for genes that, when knocked out, produced a bone phenotype and (E) human
228 monogenic bone disease genes. Red line in each panel represents Padj < 0.05.
229

230 **IV. New BMD GWAS associations further support the purple module as a core gene**
231 **module**

232 While we were analyzing the Kemp *et al.* GWAS data, an extension of this study, with a
233 significantly increased eBMD sample size, was published ("Morris *et al.* GWAS") [14]. The Estrada

et al. (N=32,961) and Kemp *et al.* (N=142,487) GWASs identified 56 and 307 conditionally independent associations, respectively [8,9]. In comparison, the Morris *et al.* GWAS (N=426,824) identified 1103 eBMD associations; an increase of over 3.5-fold [14]. The associations identified in the Morris *et al.* GWAS overlapped 1581 genes, as compared to 789 in the Estrada *et al.* and Kemp *et al.* GWASs (**Supplemental File 9**). Assuming the genetic architecture of BMD is consistent with the omnigenic model, we expected the inclusion of the Morris *et al.* GWAS data to increase the number of modules enriched for GWAS implicated genes. Consistent with this hypothesis, the number of modules enriched for GWAS-implicated genes doubled (N_{Kemp} = 13, N_{Morris} = 26) using the Morris *et al.* GWAS (**Figure 3A**) (**Supplemental File 10**). As observed in the first analysis, most (18/26, 69%) of the new modules enriched for GWAS-implicated genes were also enriched for partitioned BMD heritability (**Supplemental File 11 and Figure 3C**). These new modules were enriched for genes involved in general biological processes such as RNA splicing (brown module, Padj = 4.0×10^{-11}), cell junctions (floralwhite module, Padj = 6.2×10^{-3}), cell motor activity (orange, Padj = 6.6×10^{-3}), the cell cycle (lightgreen, Padj = 3.2×10^{-4}), ER to Golgi trafficking (salmon, Padj = 1.8×10^{-2}), and the glycolytic process (red, Padj = 1.1×10^{-13}), and not processes specific to osteoblast activity and/or mineralization **(Supplemental File 2)**.

Similar to the analysis of the Kemp *et al.* data, the purple module was among the most enriched for GWAS implicated genes (OR = 2.67, Padj = 3.4×10^{-11}) (**Figures 3A**) and BMD heritability captured (OR = 5.8, Padj = 4.7×10^{-6}) (**Figures 3B**). Using the Estrada *et al.* and Kemp *et al.* GWAS, the purple module contained 45 genes implicated by GWAS (OR = 3.15, Padj = 2.3×10^{-8}) (5.7% of GWAS-implicated genes; 8.9% of purple module genes) and explained 27% of the SNP-heritability (h_{g2}) in the study, or 4.6% of the total heritability. Using the Morris *et al.* GWAS, the number of purple module genes implicated by GWAS increased to 77 (OR = 2.7, Padj = 3.4×10^{11}) (4.9% of GWAS-implicated genes; 15.2% of purple module genes) explaining 25.3% of the h_{g2}, or 5.4% of the total heritability. Additionally, the purple

module was still the only one correlated with *in vitro* mineralization (**Figure 3D**), the most significantly enriched for genes eliciting a bone phenotype when knocked-out in mice **(Figure 3E**), and human monogenic bone disease genes (**Figure 3F**). These data indicate that even with a significant increase in the number of GWAS-implicated genes included in the analysis, the purple module is the only one enriched for genes with core like properties.

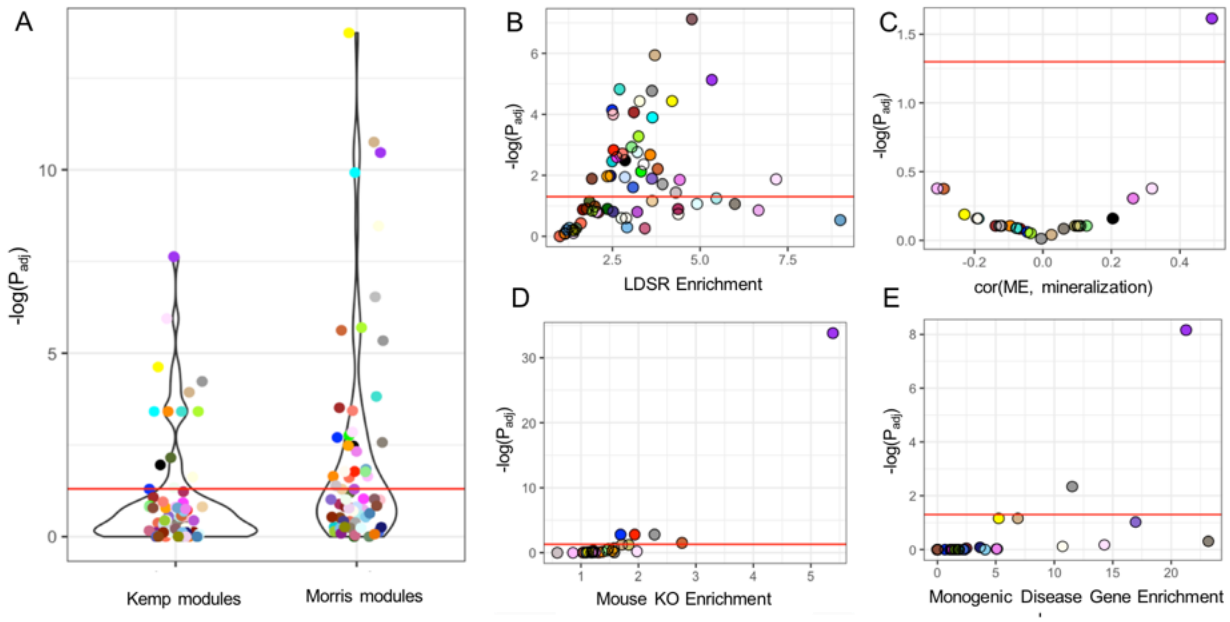

Figure 3. *The purple module was the only core module after increasing the number of analyzed GWAS associations by 3.5-fold.* (A) A greater number of modules were identified as enriched for GWAS implicated genes in the Morris *et al.* GWAS versus the Kemp *et al.* GWAS. (B) Module enrichments for partitioned BMD heritability for each module determined using stratified LD score regression. (C) Correlation between each module eigengene and *in vitro* mineralization. (D) Module enrichments for genes that, when knocked out, produced a bone phenotype and (E) human monogenic bone disease genes. Red line in each panel represents Padj < 0.05.

V. The purple module contains genes belonging to one of two distinct transcriptional

programs across osteoblast differentiation

The purple module was enriched for GO categories important for the function of osteoblasts. Consistent with this observation, it contained many genes known to play key roles in osteoblast differentiation and mineralization, including *Runx2* [13], *Sp7* [35], *Sost* [36,37], *Bglap* [38], *Alpl* [39], among many others (**Supplemental File 12**). Thus, to further investigate the purple module, we evaluated the expression of its genes with regards to osteoblast differentiation. To do this, we utilized transcriptomic profiles collected from purified osteoblasts at multiple time points across differentiation (GSE54461). Using k-means clustering, we found that the genes within the purple module clearly partitioned into two distinct transcriptional profiles with regards to differentiation (**Figure 4A,B**). We have termed these groups the Early Differentiation Submodule (EDS; high expression early and low expression late) (N=192 transcripts; 175 unique genes) and the Late Differentiation Submodule (LDS; low expression early and high expression late) (N=423 transcripts; 323 unique genes).

We assessed whether there were differences between the EDS and the LDS with regard to network parameters and their enrichment for functional annotations seen in the purple module. We first looked at intramodular connectivity, measured by module membership (correlation between the expression of each gene and the module eigengene). On average, LDS genes had higher module membership scores than EDS genes ($P = 3.0 \times 10^{-4}$) (**Figure 4C**), suggesting they may play more critical roles in the context of overall module behavior. Additionally, the LDS was more significantly enriched for genes implicated by GWAS (OR = 3.0, $Padj = 5.2 \times 10^{-10}$), osteoblast relevant GO terms (e.g. “ossification“ ($Padj = 3.24 \times 10^{-14}$), skeletal development” ($Padj = 9.6 \times 10^{-11}$), “osteoblast differentiation” ($Padj = 1.4 \times 10^{-4}$), and “biomineral tissue development” ($Padj = 4.1 \times 10^{-6}$), genes that when knocked-out result in a bone phenotype (OR = 7.3, $Padj = 1.1 \times 10^{-33}$) and monogenic bone disease genes (OR = 33.2, $Padj = 8.4 \times 10^{-11}$) (Figure 4D). As one would expect based on their higher expression later in differentiation, many of the most well-known regulators of mineralization, such as *Phospho1* [40], *Bglap* [41],

Fam20c [42], *Mepe* [43], *Phex* [44], to name a few, were members of the LDS (**Supplemental File 12**). These observations, together with the fact that LDS genes are expressed at high levels during late differentiation, coincident with when the osteoblasts are actively mineralizing, suggest that LDS contains genes with core-like properties specific for the process of mineralization. For all downstream analyses we focused on the LDS.

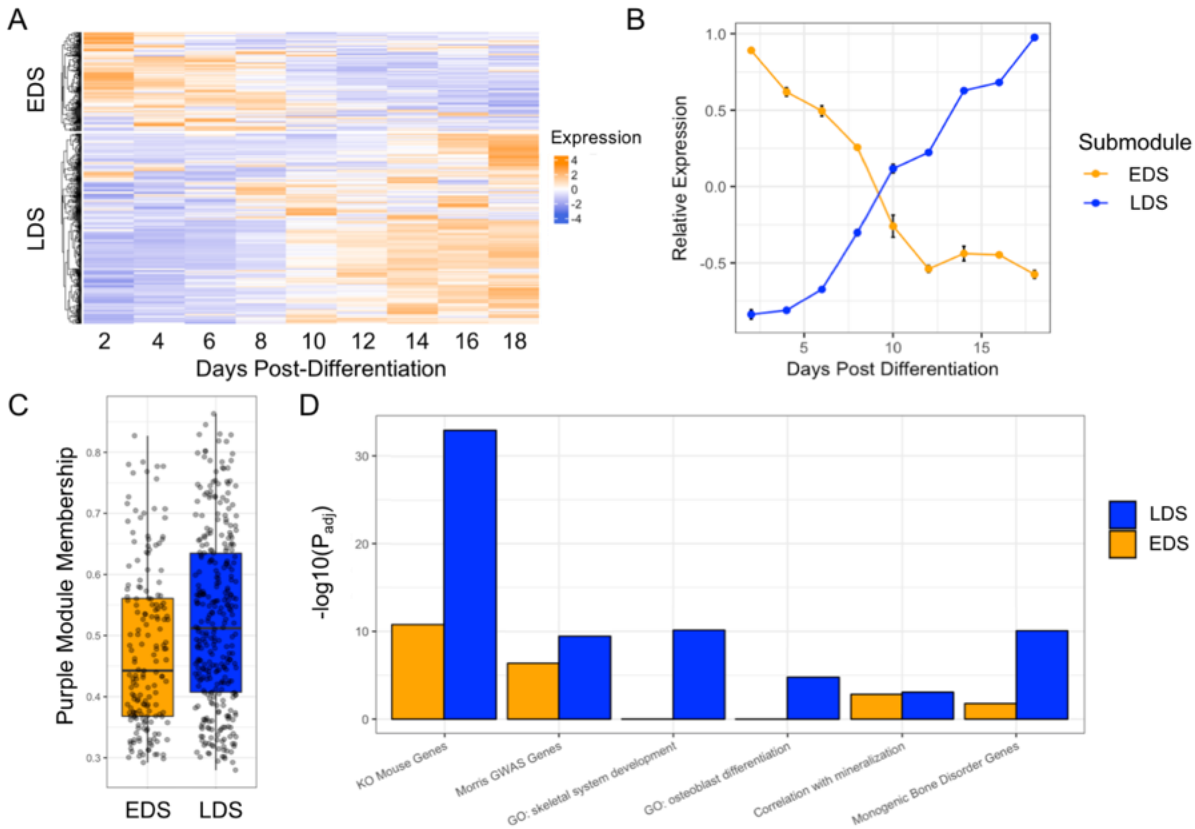

Figure 4. *The purple module consists of genes representing two distinct transcriptional profiles across osteoblast differentiation, one of which, the late differentiation submodule (LDS), is more enriched for genes with properties consistent with core genes for mineralization.* (A) Purple module genes show two distinct patterns of expression across differentiation, (B) Genes in cluster 1 (or the early differentiation submodule; EDS; N=175 genes) are expressed high early in osteoblast differentiation. Genes in cluster 2 (or the late differentiation submodule; LDS; N=323 genes) are expressed high late in osteoblast differentiation. (C) LDS genes have a significantly higher purple module membership score ($P = 3.0 \times 10^{-4}$). (D) The LDS is more

316 significantly enriched than the EDS for genes implicated by BMD GWAS in humans, associated
317 with GO terms for bone development, for genes that when knocked out, produce a bone
318 phenotype, and for genes involved in monogenic bone disorders.
319
320 **VI. BMD-associated variants in GWAS loci harboring LDS genes overlap active regulatory**
321 **elements in osteoblasts**
322 Based on the fact that the LDS is enriched for genes involved in osteoblast
323 differentiation and that mineralization is fundamental in the regulation of BMD, we anticipate that
324 many of the genes in the LDS are true core genes and causal genetic drivers of BMD. If true,
325 then BMD-associated variants in associations harboring LDS genes should regulate the
326 expression of LDS genes in osteoblasts. To test this, we utilized histone modification data from
327 the Roadmap Epigenome Project [45]. In the Morris *et al.* BMD GWAS, 48 LDS genes overlapped
328 84 associations (7.6% of the 1103 total; a subset of LDS genes overlapped multiple clustered
329 associations). For each of the 84 independently associated lead (i.e., most significant) SNPs,
330 we analyzed histone modifications across the osteoblast genome and observed that they were
331 more likely to overlap regions marked by modifications associated with active regulatory
332 elements such as H3K4me1 (2.8x enrichment, $P < 1 \times 10^{-3}$), H3Kme2 (3.2x enrichment, $P < 1 \times$
333 10^{-3}), H3K4me3 (3.8x enrichment, $P < 1 \times 10^{-3}$), and H3K27ac (2.6x enrichment, $P < 1 \times 10^{-3}$)
334 relative to 1000 sets of random SNPs matched for allele frequency and distance from a
335 transcription start site (**Figure 5**). Additionally, we observed depletion of LDS SNPs in
336 heterochromatic regions, marked by H3K9me3 (0.14x depletion, $P < 1 \times 10^{-3}$).
337 To determine if the enrichments were specific to osteoblasts, we calculated the ratio
338 between the LDS BMD set overlap and the mean random set overlap across all 129 Roadmap
339 tissues and cell-types. For all activating marks (H3K27ac, H3K4me1, H3K4me2, H3K4me3)
340 osteoblasts were in the top 10% when tissues were ranked based on the overlap ratio
341 (**Supplemental File 13**). The tissues for which the random sets had a higher ratio included cell

342 types within the same lineage as osteoblasts, such as mesenchymal stem cell (MSC) derived
343 chondrocytes and other MSC-derived tissues including adipose and skeletal muscle. These
344 data support the premise that loci harboring LDS genes impact BMD through the regulation of
345 gene expression in osteoblasts, further supporting the causality of LDS genes.

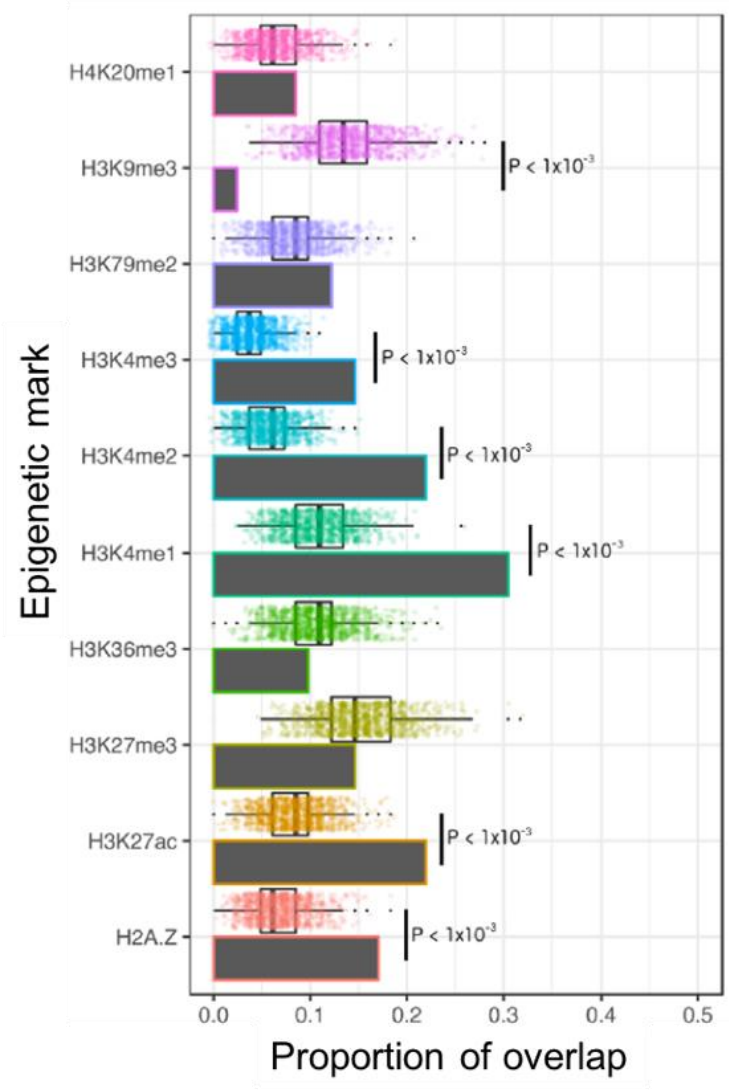

346

347 **Figure 5.** *Lead SNPs for GWAS associations harboring LDS genes overlap active regulatory*
348 *elements in osteoblasts.* Grey bars represent the proportion of LDS SNPs (n = 84) that overlap
349 each of the epigenetic marks measured in osteoblasts. Box and dot plots represent the
350 proportion of each set of random SNPs (N = 1000) (matched to the LDS SNPs for MAF and
351 distance from TSS) overlapping each epigenetic mark measured in osteoblasts.

352

353 **VII. LDS genes *CADM1*, *B4GALNT3*, *DOCK9*, and *GPR133* are novel genetic determinants**
354 **of BMD**

355 The overarching goal of this study was to identify causal genes from a module enriched
356 for genes with core-like properties underlying BMD GWAS associations. As described above, 48
357 (14.9%) LDS genes overlapped an eBMD GWAS association from the Morris *et al.* study. To
358 further identify those with strong evidence of being causal, we utilized expression quantitative
359 trait locus (eQTL) data from the Gene Tissue Expression (GTEx) project to identify local eQTL
360 colocalizing with BMD associations [46]. We also used total body BMD data on LDS gene
361 knockouts collected as part of the International Mouse Phenotyping Consortium (IMPC) [27].
362 Together, these data allowed us to directly link BMD associated variants to LDS genes and LDS
363 genes to pathways regulating BMD. We performed a colocalization analysis for each
364 eQTL/BMD association pair for all 48 genes in 48 GTEx tissues and identified 12 LDS genes
365 with colocalizing eQTL (PP4>0.7) (**Supplemental File 14 and Figures 6A, B, C, and D**). We
366 also queried each of 12 LDS genes with a colocalizing eQTL and found that BMD had been
367 measured by the IMPC in 5 mutants. Of these, four genes (*Cadm1*, *B4galnt3*, *Dock9*, and
368 *Adgrd1*) had significantly altered total body BMD (Padj < 0.05) (**Supplemental File 15 and**
369 **Figures 6E, F, G and H**). For *Cadm1* and *Dock9* the direction of effect inferred from the
370 eQTL/BMD association matched the direction of the effect observed in the mouse knockout;
371 however, for *B4galnt3* and *Adgrd1* the directions did not match (**Supplemental File 15**).
372 Lastly, we evaluated network parameters of *Cadm1*, *B4galnt3*, *Dock9* and *Adgrd1*. We
373 observed that *Cadm1* and *B4galnt3* were ranked in the top 20 based on LDS connectivity
374 (**Supplemental File 12**). In fact, *Cadm1* was the 2nd most highly connected gene. Together,
375 the four genes had, on average, higher module membership than the average LDS gene (0.72
376 vs. 0.52; P = 0.002). In support of the importance of connectivity in the LDS, we observed that
377 more highly connected LDS genes were more likely (P=0.008) to overlap a BMD GWAS locus

(**Supplemental Figure 3A**) and there was a strong positive correlation between connectivity and *in vitro* mineralization for all LDS genes (r = 0.71, P< 2.2 x 10^{-16}) (**Supplemental Figure 3B**). These data suggest that connectivity is an important feature of the LDS and a strong proxy for biological importance. Furthermore, these data strongly support *CADM1*, *B4GALNT3*, *DOCK9* and *ADGRD1* as genetic drivers of BMD in humans.

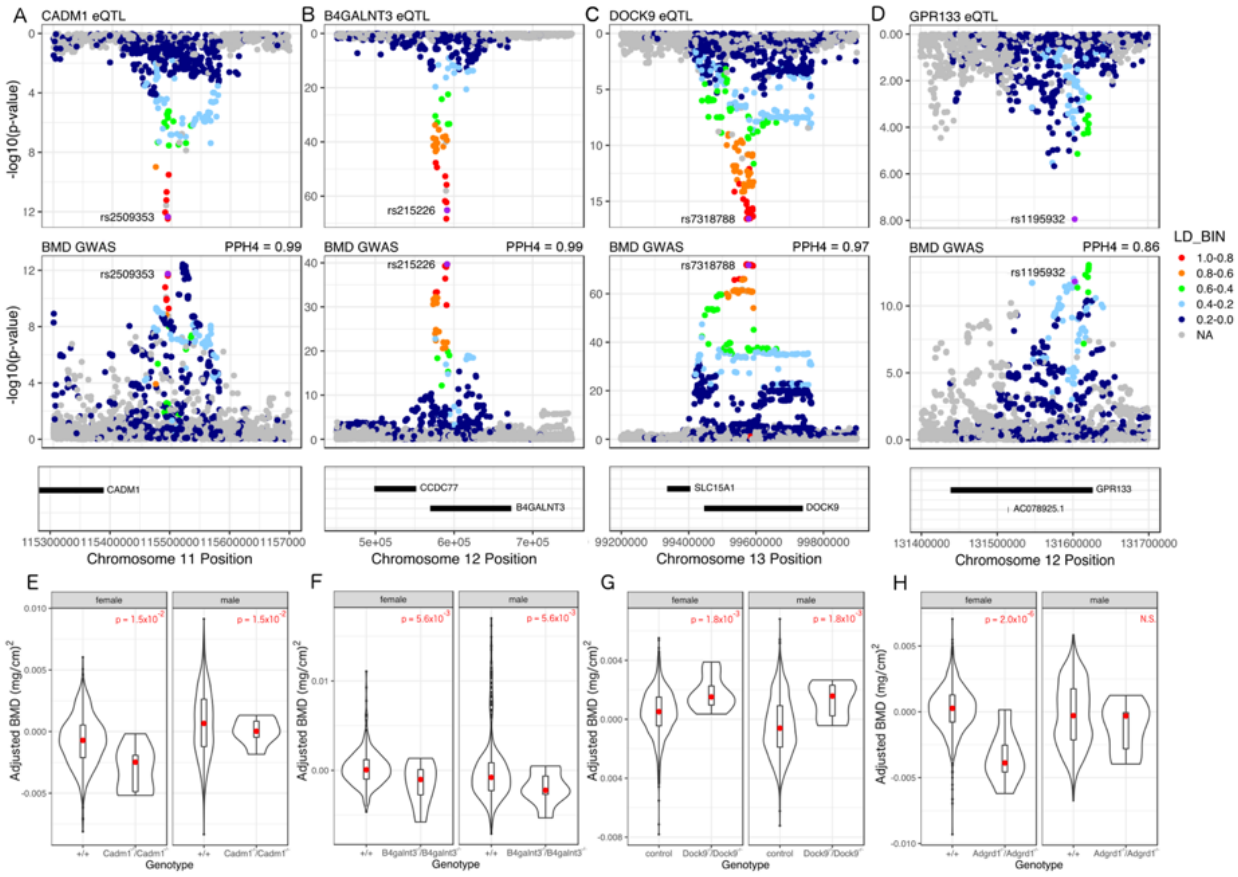

Figure 6. *CADM1, B4GALNT3, DOCK9, and ADGRD1* (aka *GPR133*) *are novel genetic regulators of BMD.* (A-D) All four genes have an eQTL in at least one tissue in the GTEx database that colocalizes with a proximal BMD GWAS association. (E-H) Knockout mice from the KOMP for each gene exhibit altered BMD.

Discussion

Osteoporosis is an increasingly common disease associated with reduced BMD and negative health outcomes, namely fracture [1]. Despite its significant genetic component, we do not fully understand the genes and mechanisms that influence osteoporosis and its determinants, such as BMD. Moreover, current therapeutics for osteoporosis have been associated with rare side effects, leading to decreased compliance [47]. Identification of the causal genes with core-like properties that regulate BMD will help us to further understand the etiology of osteoporosis and lead to the development of novel therapeutics. In this study, we identified the LDS, a co-expression submodule enriched for genes with core-like properties influencing BMD, by integrating a cell- and timepoint-specific co-expression network with the results of BMD GWAS. We then used this information to identify four LDS genes that overlapped GWAS loci, had colocalizing eQTL, and altered BMD in knockouts, suggesting they are causal for their respective BMD GWAS association.

In this work, we hypothesized that the genes underlying BMD GWAS associations are not created equal with respect to “biological importance” or membership in pathways with direct impacts on bone mass. Substantial prior evidence supports this prediction [48,49]and it is one of the primary tenets of the omnigenic model [11,12]. Identification of genes whose activity or function is more proximal to BMD is important for a number of reasons. First, the identification of genes with core-like properties has the potential to identify critical new players in pathways known to directly impact bone and to uncover new processes essential to skeletal growth and maintenance. Second, it provides a way to prioritize hundreds of BMD GWAS loci for further investigation. Third, based on their central role in the regulation of BMD, it is logical to use the concept of a core gene as a way to prioritize gene discovery in the context of selecting promising new therapeutic targets for evaluation.

The omnigenic model uses a strict statistical definition to define core genes and many

have debated the utility of this designation[11,15–17]. Some have argued that focusing on core genes underestimates the complexity of complex traits, attributing biologically nuanced diseases to a small set of genes [13]. Others have argued that the focus should not be on thoroughly defining core genes, but instead on identifying the underlying biological pathways and mechanisms [14]. In practice, it is likely that the designation of core genes follows a spectrum rather than a discrete classification. If so, then it should be possible to rank genes based on their continuous "core" attributes, which would be analogous to ranking genes based on their proximity to a disease or phenotype. In essence, that is what we have done in the current study with the goal of identifying genes on the end of the "core" attribute distribution for mineralization. Importantly, it is not likely that all genes in the LDS are causal genetic drivers or, if they are causal, it is possible that several will have few core attributes. However, based on our analysis and results, it is likely that many are causal genes that participate in "core" pathways and processes that directly impact mineralization, bone formation, and BMD.

As we have previously demonstrated [50,51], there are a number of advantages to using co-expression networks to inform GWAS. First, it allowed us to group genes across the genome based on function and pathway membership and then identify groups of functionally similar genes that had core-like properties. Second, it allowed us to predict the function of potentially casual genetic drivers of BMD. Based on the strong GO enrichments and membership of genes with well-known roles in bone formation and mineralization, it is likely that all LDS genes, including those with no known function, impact mineralization in some manner. The idea of the LDS playing a central role in bone formation was further supported by the strong overlap observed between lead BMD GWAS SNPs for associations containing LDS genes regulatory elements in osteoblasts. Third, it begins to provide a systems-level context for causal genetic drivers. Once genes underlying GWAS loci are identified it is then important to begin to understand their role in complicated cellular networks, defining how a set of genetic variants may converge on multiple genes all involved in a particular process. We can use the LDS to

443 begin to identify sets of variants that all work to influence genes which impact mineralization and
444 the hierarchy of relationships between these genes.

445 This work extends our use of co-expression networks to inform GWAS. Previously, we
446 used a network generated using cortical bone expression profiles from the Hybrid Mouse
447 Diversity Panel to identify two "osteoblast" modules (enriched for genes involved in osteoblast
448 differentiation and function) enriched for genes implicated by BMD GWAS. We used these
449 modules to identify 35 genes potentially causal for GWAS loci, including two (*MARK3* and
450 *SPTBN1*) that we experimentally validated their involvement in BMD. Comparing the two
451 modules to the LDS we observed a modest overlap (96 of 323 genes; 29.7%), even though they
452 both demonstrated a strong "osteoblast" enrichment signature. While a number of differences
453 (microarray vs. RNA-seq transcriptomic data, different mouse populations, etc.) confound the
454 interpretation of the seemingly low overlap, it is likely due in large part to our use of osteoblast-
455 specific network capturing the transcriptome at peak mineralization instead of the whole bone
456 tissue representing a small number of osteoblasts.

457 We provided strong supporting evidence that four LDS genes (*CADM1*, *B4GALNT3*,
458 *DOCK9* and *GPR133*) are novel regulators of BMD and causal for their respective GWAS
459 association. Prior to this study, none of these genes had been directly connected to the
460 regulation of BMD. *CADM1* (Cell Adhesion Molecule 1) is a ubiquitously expressed cell
461 adhesion molecule involved in many biological processes, including cancer, spermatogenesis,
462 and neuronal/mast/epithelial cell function[52–54] that had been implicated in osteoclast proliferation
463 and activity[55] and as an osteoblast-specific marker in the context of osteosarcoma[56,57].
464 *B4GALNT3* (Beta-1,4-N-Acetyl- Galactosaminyltransferase 3) is a glycosyltransferase that
465 transfers N-acetylgalactosaine (GalNAc) onto glucosyl residues, thus forming N,N-prime-
466 diacetyllactoseadiamine (LacdiNAc), which serves as a terminal structure of cell surface N-
467 glycans that contributes to cell signaling [51,52]. *B4GALNT3* is expressed in bone and associated
468 with circulating levels of sclerostin [53-55]. *DOCK9* (Dedicator of Cytokinesis 9) is a guanine

nucleotide-exchange factor (GEF) that activates Cdc42[58], which has been shown to regulate osteoclast differentiation and ossification [57,58]. *GPR133* (Adhesion G Protein-Coupled Receptor D1) is a G protein-coupled receptor that participates in cell-cell and cell-matrix interactions [59]. Our results demonstrate the utility of the LDS in broadening our understanding of the molecular and genetic basis of BMD.

Our study is not without limitations. First, we used gene expression data from the mouse as a discovery platform, however this may limit the translational applications of the work due biological differences and missing homologs between mouse and human. Secondly, this was not a comprehensive study of the genetic effects driving osteoporosis, because we focused exclusively on the contributions of just one cell type, bone-forming osteoblasts. In future work, this approach could also be applied to other bone cell types. For example, one could use *in vitro* measures of osteoclast activity as a filter to identify groups of genes influencing bone resorption, and ultimately BMD. Finally, the eQTL comparisons made in this study were not derived from expression data in bone tissue, as bone tissue expression was not measured in the GTEx project. While we identified colocalizing eQTL in other tissues, these eQTL may be irrelevant to BMD or the direction of eQTL effects in non-bone tissues may not reflect the direction of effect in osteoblasts.

While we identified four novel regulators of bone mineral density, there is still much to be gleaned from the late differentiation submodule. The LDS is a promising resource for two key applications: (1) causal gene discovery and functional follow up and (2) studying the impact of genetic variation on biological networks and complex phenotypes. There are still many genes with no known connection to BMD in the LDS that are likely important to osteoblast biology and mineralization. Additionally, the LDS is not just a list of candidate genes; it also provides insight into the molecular hierarchy driving osteoblast differentiation and mineralization, which can demonstrate how genetic variation impacts biological networks. The network topology of the LDS can also be used to infer the causal relationships between genetic variants and the many

genes that influence osteoblast activity. Moving forward, the LDS can serve as a platform for the identification of novel determinants of BMD and for furthering our understanding of the nuanced relationship between genetic variation, molecular phenotypes, and complex traits.

In summary, we have used an integrative, network-based method to identify core genes for the process of mineralization and BMD. While the definition of a core gene is still open to debate, we found the expected properties of core genes are effective lenses through which to contextualize GWAS associations. Integrating gene co-expression networks, GWAS data, *in vitro* and *in vivo* phenotypic data reflecting "core" properties, and eQTL information has led us to a more complete understanding of the biology and genetics of BMD.

Methods

RNA-seq: Neonatal collaborative cross heads were received from the University of North Carolina. At UNC, neonatal (3-5 days) collaborative cross mice were euthanized by CO_2, decapitated onto paper towels soaked in 70% ethanol, and placed in cold PBS on ice for overnight shipping. Once received, calvaria were dissected, paying special attention to brain and interparietal bone removal. Isolated calvaria were placed in 24 well plates containing 0.5 mL of digest solution (0.05% trypsin and 1.5 U/ml collagenase P) and incubated on a rocking platform at 37 degrees during six, fifteen-minute digestions in 0.5 mL of digestion solution. Fraction 1 is discarded and fractions 2-6 are collected. Fractions 2-6 are added to an equal volume of cold plating media (89 mL DMEM, 1 mL 100x Pen/Strep solution, and 10 mL Lot tested FBS). The resulting cells are filtered using a 70-100 mm cell strainer to remove clots, centrifuged at 1000 rpm for 5 minutes and re-suspended in 0.5 ml plating media. The resulting cells are plated in a T25 flask. 24 hours later, cells are washed with PBS, treated with trypsin, counted, and plated at a density of $1.5x10_5$ cells per well in a 12-well plate, and allowed to grow to confluence for 48 hours. After 48 hours of growth, cells are switched to differentiation media (10 mL lot tested FCS, 1 mL 100x Pen/Strep solution, 283.8 uL ascorbic acid (0.1 M), 400 uL B-

glycerol phosphate (1 M), and 88.3 mL alpha-MEM per 100 mL) and allowed to differentiate for 10 days. On day 10, total RNA was extracted from the mineralized cultures using *mir*Vana RNA isolation kit (ThermoFisher Scientific).

RNA-Seq libraries were constructed from 200 ng of total RNA using Illumina TruSeq Stranded Total RNA with Ribo-Zero Gold sample prep kits (Illumina, Carlsbad, CA). Constructed libraries contained RNAs >200 nt (both unpolyadenylated and polyadenylated) and were depleted of cytoplasmic and mitochondrial rRNAs. An average of 39.7 million 2 x 75 bp paired-end reads were generated for each sample on an Illumina NextSeq 500 (Illumina, Carlsbad, CA). FastQC was used to evaluate the quality of the reads, and all samples passed the QC stage [59]. Reads were mapped to the eight collaborative cross founder transcriptomes based on build mm9 using Bowtie, and quantified using EMASE [60]. EMASE output transcript level expression estimates calculated by assigning multi-mapping reads across the genome using and expectation-maximization algorithm to allocate reads that differentiate between genes, then isoforms of a gene, and then alleles.

WGCNA network construction: Estimated transcript count data was used as the basis for co-expression network construction. We removed transcripts with less than an average tpm <= 0.3 tpm across all samples, resulting in 29,000 transcripts used to construct the network. We used a variance stabilizing transformation from the DESeq2 package that decouples the variance from the mean [61]. Next, we used PEER in order to remove latent confounding batch effects from our data [62]. As per PEER recommendations, we estimated PEER factors equal to one quarter of the number of samples (N = 24) and included covariates in the calculation. We carried out the downstream analysis with the residual values from PEER transformation. Finally, we used quantile normalization to match the distribution of each of the samples in the analysis.

The resulting expression data was used to construct a signed, weighted gene co-expression network using the weighted gene co-expression network analysis (WGCNA)

package [63]. There were no evident outliers from the hierarchical clustering analysis. The pickSoftThreshold() function from the wgcna package was used to determine the power used to calculate the network. The minimum power value that had an R_2 >= 0.9 for the scale-free topology model fit was used, and the network was calculated using a power of 9. We then used the blockwiseModules() function to construct a signed network with a merge cut height of 0.15, and a minimum module size of 20 genes. Using WGCNA, we constructed a signed network composed of 65 modules of co-expressed genes, with an average of 292 genes per module.

Gene Ontology Analysis: For those modules that were enriched for BMD GWAS genes, we conducted gene ontology analysis to identify the functional categories represented by each module. Using the ToppFun tool on the ToppGene site, we identified the significantly enriched categories for GO molecular functions, GO biological processes, GO cellular components, human and mouse phenotypes, and pathways [64]. The significance cutoffs reported for these enrichments were Benjamini & Hochberg corrected FDR q-values.

Creating BMD GWAS list: In order to identify co-expression modules enriched for BMD GWAS genes, we identified all genes overlapping a BMD GWAS locus using the 2012 and 2017 BMD GWAS [8,9]. For each BMD locus, a bin was defined by the furthest upstream and downstream SNPs with LD >= 0.7 as calculated from the European populations in the 1000 genomes phase III data identified using the LDLink LDProxy tool [65]. Then, using the Genomic Ranges tool, we identified all genes from the GRCh37/hg19 Ensembl gene set overlapping a BMD GWAS bin [66,67]. If not gene intersected a bin, we identified the nearest upstream and downstream genes from the bin. The Estrada GWAS resulted in 179 genes and the eBMD GWAS resulted in 701 genes, resulting in a list of 731 unique genes. We converted the list of human genes to mouse homologs.

572

573 **BMD GWAS gene enrichment:** In order to identify modules of genes enriched for GWAS
574 genes, we used a fisher's exact test to measure the statistical significance of the representation
575 of GWAS genes in each module. We then applied a Bonferroni correction to correct for testing
576 the enrichment of all 65 modules, and applied a significance cutoff of 0.05 to the adjusted p-
577 values, resulting in 13 modules of genes enriched for 2012 and 2017 GWAS genes, and 26
578 modules of genes enriched for 2012, 2017, and 2018 GWAS genes.

579

580 **LD Score Regression:** In order to evaluate the relevance of the BMD GWAS gene enriched
581 modules we calculated the partitioned heritability of the SNPs in the regions surrounding the
582 genes in each module. We used the LD score regression method, which takes gene lists as an
583 input and returns the enrichment of the associated SNP set for heritability for the tested trait. For
584 each set of modules we tested using this method, we corrected the enrichment p-values for
585 multiple testing using a Bonferroni correction, and applied a p-value cutoff of 0.05 to the
586 adjusted p-values.

587

588 ***In vitro* mineralization measurement and correlation:** In order to identify the modules of
589 coexpressed genes with patterns of expression correlated with mineralization, we measured *in*
590 *vitro* mineralization in osteogenic cells from the calvaria of 42 strains of collaborative cross mice.
591 After 10 days of differentiation and mineral production, cells are washed with PBS and treated
592 with 10% NBF (1 mL per well) and incubated at room temperature for 15 minutes. The NBF is
593 removed and cells are washed with H_2O (1mL x 2). Next, wells are stained with alizarin red (0.5
594 mLs, 40 mM @ pH 5.6) for 20 minutes on a shake plate at 120 rpm. Alizarin red stain is then
595 removed, and cells are washed 5 times with deionized H_2O for 5 minutes on a shake plate at
596 180 rpm. Once rinsed, the mineralized wells are scanned, and .tiff images are retained to

extract geometric parameters of the mineral deposits. After imaging, the wells are de-stained by incubation with 5% perchloric acid (1 mL) at room temperature for 5 minutes while shaking at 120 rpm. Eluent is collected and read at 405 nm. The levels of *in vitro* mineralization varied significantly across the population, with a 63-fold change from the highest to lowest mineralization samples (max_mmAR = 2.995993, min_mmAR = 0.04719).

In this population, *in vitro* mineralization had a heritability of 47.8%($p=1.8x10^{-46}$), indicating that the between-strain variation is larger than the within strain variation and that there is a genetic contribution to the process of mineralization. Using the WGCNA package, the eigengene of each module was calculated, and the correlation between the eigengene and the in vitro mineralization phenotype was calculated using the cor() function in R. The p-values associated with the correlation between the module eigengenes and *in vitro* mineralization were corrected for multiple testing using a Bonferroni correction and a p-value cutoff of 0.05 was applied to the adjusted p-values.

Module enrichment for genes with associated bone phenotypes and monogenic bone disease: In order to identify modules of coexpressed BMD GWAS genes that are enriched for genes with bone phenotype annotations, we curated a list of genes which produce a bone phenotype when knocked out. We used four databases of gene perturbations that result in bone phenotypes, including genes annotated with a bone phenotype in the Mouse Genome Informatics database (MGI), the Origins of Bone and Cartilage Disease (OBCD) database, the International Mouse Phenotyping Consortium (IMPC), and the Bonebase Database [26–29]. Specifically, we pulled BMD, altered bone morphology, altered bone cell activity, changes in ossification or mineralization, or association with a known bone disease from the MGI database. The OBCD database contained genes with changes in bone mineral content (BMC), bone volume fraction (BV/TV), and BMD of the femur and BMD of the vertebra. We mined the IMPC database for any genes with altered BMD, and we pulled all Bonebase genes with altered

BV/TV in the femur or vertebra. This resulted in a list of 923 unique "bone" genes (**Supplemental File 7**).

We also curated a list of genes associated with monogenic bone disorders using a literature review, specifically focusing on genes that disrupt osteoblast function, leading to monogenic bone disorders [30–34]) (**Supplemental File 8**). We used a fisher's exact test to measure the statistical significance of the representation of genes with associated mouse knockout bone phenotypes and monogenic bone disease in each module. We then applied a Bonferroni correction to correct for testing the enrichment of all 13 or 26 modules and applied a significance cutoff of 0.05 to the adjusted p-values.

Clustering analysis in osteoblast differentiation gene expression data: We investigated the expression profiles of all purple module genes in the context of differentiation. Using gene expression data from osteoblasts throughout differentiation (Series GSE54461), we used k-means clustering to identify differentiation-related transcriptional programs in the purple module. We tested k = 1:5, and found two robust clusters of genes within the purple module. Enrichment analysis of the two clusters in all function categories were conducted as described above.

Epigenetic enrichment analysis for LDS BMD GWAS associations: For BMD GWAS lead SNP (and proxies with LD >= 0.7) overlapping an LDS gene (n = 84), GenomicRanges [66] was used to calculate the proportion of lead SNPs overlapping regions marked by epigenetic modifications, including H3K4me1, H3K4me2, H3K4me3, H3K9me3, H3K27ac, H3K27me3, H3K26me3, H3K79me2 and H4K20me1, and histone H2AZ from the Roadmap Project [45]. Using the GenomicRanges function findOverlaps(), we quantified the overlap between the LDS-associated lead SNPs and each epigenetic mark. To assess the enrichment of this overlap, we compared against 1000 sets of control SNPs (n = 84). We chose sets of control SNPs that were

within +/- 20% of the mean distance from a transcription start site for the BMD GWAS lead SNPs, and within +/- 20% of the mean minor allele frequency of the BMD GWAS lead SNPs. P-values were calculated by taking the proportion of random sets of SNPs with a more extreme enrichment in the tail of the distribution with which we are comparing our experimental proportion. If the experimental proportion is more extreme than any measured random set, the p-value is reported as $< 1x10^{-3}$. This same procedure was used to evaluate the tissue specificity for each mark. For each mark, the overlap with the LDS BMD SNP set and the 1000 random SNP sets were computed and the ratio between the proportion of overlapping LDS BMD SNPs and the mean proportion of overlapping random SNPs was computed. Higher ratios indicated greater enrichment of the LDS BMD SNPs over random SNPs with a given mark in a given tissue.

Colocalization analysis: For each gene in the LDS that overlapped a BMD GWAS association from the Morris *et al.* study, eQTL from all GTEx tissues were identified [10,46]. Using the coloc package, we assessed the potential for colocalization between the QTL for BMD and the proximal cis-eQTL [68]. Two associations were considered to colocalize if the posterior probability of hypothesis four (PPH4), which is the probability of colocalization, is > 0.7. The RACER package to plot the two associations in a mirrorPlot [69].

Mouse phenotype statistical comparisons: Using the International Mouse Phenotyping Consortium (IMPC) database, we identified genes from the LDS that had eQTL that colocalized with BMD QTL and exhibited a difference in BMD when knocked out in mouse [27]. Using the PhenStat package, we analyzed the differences between control and knockout animals using a mixed model framework [70]. The specific equation used for each analysis are in **Supplemental File 15**.

673

674 **Network Topology Analysis:** A t-test was used to compare the module membership of the four
675 causal genes and the remainder of the LDS genes and the connectivity of the LDS genes
676 overlapping a BMD GWAS locus as opposed to those that do not. A linear model was used to
677 assess the relationship between gene connectivity and gene correlation with *in vitro*
678 mineralization.

679

680 **Acknowledgements:** Research reported in this publication was supported by the National
681 Institute of Arthritis and Musculoskeletal and Skin Diseases of the National Institutes of Health
682 under Award Number R01AR064790 to C.L.A-B. and C.R.F. O.L.S. was supported by a Wagner
683 Fellowship from the University of Virginia. The Genotype-Tissue Expression (GTEx) Project was
684 supported by the Common Fund of the Office of the Director of the National Institutes of Health,
685 and by NCI, NHGRI, NHLBI, NIDA, NIMH, and NINDS. The data used for the analyses
686 described in this manuscript (v7) were obtained from: the GTEx Portal on 01/11/2018. The
687 International Mouse Phenotyping Consortium is partially funded by the NIH Knockout Mouse
688 Programme (KOMP) project and the IMPC informatics and the data portal are supported by NIH
689 grant U54 HG006370.

690

691

692

693

694

695

696

References:

1. Black, D. M. & Rosen, C. J. Clinical Practice. Postmenopausal Osteoporosis. *N. Engl. J. Med.* 374, 254–262 (2016).
2. Johnell, O. & Kanis, J. A. An estimate of the worldwide prevalence and disability associated with osteoporotic fractures. *Osteoporos. Int.* 17, 1726–1733 (2006).
3. Ralston, S. H. & Uitterlinden, A. G. Genetics of osteoporosis. *Endocr. Rev.* 31, 629–662 (2010).
4. Zheng, H.-F., Spector, T. D. & Richards, J. B. Insights into the genetics of osteoporosis from recent genome-wide association studies. *Expert Rev. Mol. Med.* 13, e28 (2011).
5. Ralston, S. H. & de Crombrugghe, B. Genetic regulation of bone mass and susceptibility to osteoporosis. *Genes Dev.* 20, 2492–2506 (2006).
6. Sabik, O. L. & Farber, C. R. Using GWAS to identify novel therapeutic targets for osteoporosis. *Transl. Res.* (2016). doi:10.1016/j.trsl.2016.10.009
7. Hsu, Y.-H., Farber, C. R. & Kiel, D. P. Genetic determinants of bone mass and osteoporotic fracture. *Principles of Bone Biology* 1615–1630 (2020). doi:10.1016/b978-0-12-814841-9.00068-3
8. Estrada, K. *et al.* Genome-wide meta-analysis identifies 56 bone mineral density loci and reveals 14 loci associated with risk of fracture. *Nat. Genet.* 44, 491–501 (2012).
9. Kemp, J. P. *et al.* Identification of 153 new loci associated with heel bone mineral density and functional involvement of GPC6 in osteoporosis. *Nat. Genet.* 49, 1468–1475 (2017).
10. Morris, J. A. *et al.* An Atlas of Human and Murine Genetic Influences on Osteoporosis. *bioRxiv* 338863 (2018). doi:10.1101/338863
11. Boyle, E. A., Li, Y. I. & Pritchard, J. K. An Expanded View of Complex Traits: From Polygenic to Omnigenic. *Cell* 169, 1177–1186 (2017).
12. Liu, X., Li, Y. I. & Pritchard, J. K. Trans Effects on Gene Expression Can Drive Omnigenic Inheritance. *Cell* 177, 1022–1034.e6 (2019).
13. Komori, T. Regulation of Osteoblast Differentiation by Runx2. *Advances in Experimental Medicine and Biology* 43–49 (2009). doi:10.1007/978-1-4419-1050-9_5
14. Morris, J. A. *et al.* An atlas of genetic influences on osteoporosis in humans and mice. *Nat. Genet.* 51, 258–266 (2019).
15. Boyle, E. A., Li, Y. & Pritchard, J. K. The omnigenic model: Response from the authors. *J. Psychiatry Brain Sci.* 2, S8 (2017).
16. Wray, N. R., Wijmenga, C., Sullivan, P. F., Yang, J. & Visscher, P. M. Common Disease Is More Complex Than Implied by the Core Gene Omnigenic Model. *Cell* 173, 1573–1580 (2018).
17. Cox, N. J. Comments on Pritchard Paper. *Journal of Psychiatry and Brain Science* 2, S5 (2017).
18. Mäkinen, V.-P. *et al.* Integrative genomics reveals novel molecular pathways and gene networks for coronary artery disease. *PLoS Genet.* 10, e1004502 (2014).

19. Civelek, M. & Lusis, A. J. Systems genetics approaches to understand complex traits. *Nat. Rev. Genet.* 15, 34–48 (2014).
20. Rau, C. D. *et al.* Systems Genetics Approach Identifies Gene Pathways and Adamts2 as Drivers of Isoproterenol-Induced Cardiac Hypertrophy and Cardiomyopathy in Mice. *Cell Syst* 4, 121–128.e4 (2017).
21. Kogelman, L. J. A. *et al.* Identification of co-expression gene networks, regulatory genes and pathways for obesity based on adipose tissue RNA Sequencing in a porcine model. *BMC Med. Genomics* 7, 57 (2014).
22. Eising, E. *et al.* Gene co-expression analysis identifies brain regions and cell types involved in migraine pathophysiology: a GWAS-based study using the Allen Human Brain Atlas. *Hum. Genet.* 135, 425–439 (2016).
23. Churchill, G. A. *et al.* The Collaborative Cross, a community resource for the genetic analysis of complex traits. *Nat. Genet.* 36, 1133–1137 (2004).
24. van Dam, S., Võsa, U., van der Graaf, A., Franke, L. & de Magalhães, J. P. Gene co-expression analysis for functional classification and gene–disease predictions. *Brief. Bioinform.* 19, 575–592 (2018).
25. Finucane, H. K. *et al.* Partitioning heritability by functional annotation using genome-wide association summary statistics. *Nat. Genet.* 47, 1228–1235 (2015).
26. Bolser, D. Mouse Genome Informatics (MGI, Mouse Genome Database, MGD). *Dictionary of Bioinformatics and Computational Biology* (2004). doi:10.1002/9780471650126.dob1002
27. Koscielny, G. *et al.* The International Mouse Phenotyping Consortium Web Portal, a unified point of access for knockout mice and related phenotyping data. *Nucleic Acids Res.* 42, D802–9 (2014).
28. Dyment, N. A. *et al.* High-Throughput, Multi-Image Cryohistology of Mineralized Tissues. *J. Vis. Exp.* (2016). doi:10.3791/54468
29. Freudenthal, B. *et al.* Rapid phenotyping of knockout mice to identify genetic determinants of bone strength. *J. Endocrinol.* 231, R31–46 (2016).
30. Johnson, M. L. How rare bone diseases have informed our knowledge of complex diseases. *Bonekey Rep* 5, 839 (2016).
31. Boudin, E. & Van Hul, W. MECHANISMS IN ENDOCRINOLOGY: Genetics of human bone formation. *Eur. J. Endocrinol.* 177, R69–R83 (2017).
32. Robinson, M.-E. & Rauch, F. Mendelian bone fragility disorders. *Bone* (2019). doi:10.1016/j.bone.2019.04.021
33. Marini, F. & Brandi, M. L. Genetic determinants of osteoporosis: common bases to cardiovascular diseases? *Int. J. Hypertens.* 2010, (2010).
34. Rocha-Braz, M. G. M. & Ferraz-de-Souza, B. Genetics of osteoporosis: searching for candidate genes for bone fragility. *Arch Endocrinol Metab* 60, 391–401 (2016).
35. Yoshida, C. A. *et al.* SP7 inhibits osteoblast differentiation at a late stage in mice. *PLoS One* 7, e32364 (2012).
36. Semënov, M., Tamai, K. & He, X. SOST is a ligand for LRP5/LRP6 and a Wnt signaling inhibitor. *J. Biol. Chem.* 280, 26770–26775 (2005).
37. Atkins, G. J. *et al.* Sclerostin is a locally acting regulator of late-osteoblast/preosteocyte differentiation and regulates mineralization through a MEPE-ASARM-dependent mechanism. *Journal of Bone and Mineral Research* 26, 1425–1436 (2011).

38. Nakamura, A. *et al.* Osteocalcin secretion as an early marker of in vitro osteogenic differentiation of rat mesenchymal stem cells. *Tissue Eng. Part C Methods* 15, 169–180 (2009).
39. Golub, E. E. & Boesze-Battaglia, K. The role of alkaline phosphatase in mineralization. *Curr. Opin. Orthop.* 18, 444 (2007).
40. Roberts, S., Narisawa, S., Harmey, D., Millán, J. L. & Farquharson, C. Functional involvement of PHOSPHO1 in matrix vesicle-mediated skeletal mineralization. *J. Bone Miner. Res.* 22, 617–627 (2007).
41. Neve, A., Corrado, A. & Cantatore, F. P. Osteocalcin: Skeletal and extra-skeletal effects. *Journal of Cellular Physiology* 228, 1149–1153 (2013).
42. Liu, C. *et al.* FAM20C regulates osteoblast behaviors and intracellular signaling pathways in a cell-autonomous manner. *Journal of Cellular Physiology* 233, 3476–3486 (2018).
43. Cho, Y. & Ryoo, H.-M. MEPE: A Mineralization Regulating Bone Matrix Protein. *Journal of Korean Endocrine Society* 23, 71 (2008).
44. Quarles, L. D. & Darryl Quarles, L. FGF23, PHEX, and MEPE regulation of phosphate homeostasis and skeletal mineralization. *American Journal of Physiology-Endocrinology and Metabolism* 285, E1–E9 (2003).
45. Chadwick, L. H. The NIH Roadmap Epigenomics Program data resource. *Epigenomics* 4, 317–324 (2012).
46. GTEx Consortium *et al.* Genetic effects on gene expression across human tissues. *Nature* 550, 204–213 (2017).
47. Kolata, G. Fearing drugs' rare side effects, millions take their chances with osteoporosis. *NY Times* (2016).
48. Manolio, T. A. *et al.* Finding the missing heritability of complex diseases. *Nature* 461, 747–753 (2009).
49. International Schizophrenia Consortium *et al.* Common polygenic variation contributes to risk of schizophrenia and bipolar disorder. *Nature* 460, 748–752 (2009).
50. Farber, C. R. Identification of a gene module associated with BMD through the integration of network analysis and genome-wide association data. *J. Bone Miner. Res.* 25, 2359–2367 (2010).
51. Calabrese, G. M. *et al.* Integrating GWAS and Co-expression Network Data Identifies Bone Mineral Density Genes SPTBN1 and MARK3 and an Osteoblast Functional Module. *Cell Syst* 4, 46–59.e4 (2017).
52. Wakayama, T. & Iseki, S. Role of the spermatogenic–Sertoli cell interaction through cell adhesion molecule-1 (CADM1) in spermatogenesis. *Anat. Sci. Int.* 84, 112–121 (2009).
53. Zhang, W. *et al.* CADM1 regulates the G1/S transition and represses tumorigenicity through the Rb-E2F pathway in hepatocellular carcinoma. *Hepatobiliary Pancreat. Dis. Int* 15, 289–296 (2016).
54. Cao, W., Shi, P. & Ge, J.-J. miR-21 enhances cardiac fibrotic remodeling and fibroblast proliferation via CADM1/STAT3 pathway. *BMC Cardiovasc. Disord.* 17, 88 (2017).
55. Nakamura, S. *et al.* Negative feedback loop of bone resorption by NFATc1-dependent induction of Cadm1. *PLoS One* 12, e0175632 (2017).

56. Inoue, T. *et al.* Cell adhesion molecule 1 is a new osteoblastic cell adhesion molecule and a diagnostic marker for osteosarcoma. *Life Sci.* 92, 91–99 (2013).
57. Mentink, A. *et al.* Predicting the therapeutic efficacy of MSC in bone tissue engineering using the molecular marker CADM1. *Biomaterials* 34, 4592–4601 (2013).
58. Meller, N., Irani-Tehrani, M., Kiosses, W. B., Del Pozo, M. A. & Schwartz, M. A. Zizimin1, a novel Cdc42 activator, reveals a new GEF domain for Rho proteins. *Nat. Cell Biol.* 4, 639–647 (2002).
59. Bioinformatics, B. FastQC: a quality control tool for high throughput sequence data. *Cambridge, UK: Babraham Institute* (2011).
60. Raghupathy, N. *et al.* Hierarchical analysis of RNA-seq reads improves the accuracy of allele-specific expression. *Bioinformatics* 34, 2177–2184 (2018).
61. Love, M. I., Huber, W. & Anders, S. Moderated estimation of fold change and dispersion for RNA-seq data with DESeq2. *Genome Biol.* 15, 550 (2014).
62. Stegle, O., Parts, L., Piipari, M., Winn, J. & Durbin, R. Using probabilistic estimation of expression residuals (PEER) to obtain increased power and interpretability of gene expression analyses. *Nat. Protoc.* 7, 500–507 (2012).
63. Langfelder, P. & Horvath, S. WGCNA: an R package for weighted correlation network analysis. *BMC Bioinformatics* 9, 559 (2008).
64. Chen, J., Bardes, E. E., Aronow, B. J. & Jegga, A. G. ToppGene Suite for gene list enrichment analysis and candidate gene prioritization. *Nucleic Acids Res.* 37, W305–11 (2009).
65. Machiela, M. J. & Chanock, S. J. LDlink: a web-based application for exploring population-specific haplotype structure and linking correlated alleles of possible functional variants. *Bioinformatics* 31, 3555–3557 (2015).
66. Lawrence, M. *et al.* Software for computing and annotating genomic ranges. *PLoS Comput. Biol.* 9, e1003118 (2013).
67. Hubbard, T. *et al.* The Ensembl genome database project. *Nucleic Acids Res.* 30, 38–41 (2002).
68. Giambartolomei, C. *et al.* Bayesian test for colocalisation between pairs of genetic association studies using summary statistics. *PLoS Genet.* 10, e1004383 (2014).
69. Sabik, O. L. & Farber, C. R. RACER: A data visualization strategy for exploring multiple genetic associations. *bioRxiv* 495366 (2018). doi:10.1101/495366
70. Kurbatova, N., Mason, J. C., Morgan, H., Meehan, T. F. & Karp, N. A. PhenStat: A Tool Kit for Standardized Analysis of High Throughput Phenotypic Data. *PLoS One* 10, e0131274 (2015).